Original Article

# Predicting white-matter hyperintensity progression and cognitive decline in patients with cerebral small-vessel disease: a magnetic resonance-based habitat analysis

**Xu Han[1#], Yao Wang[1#], Yuewei Chen[2], Yage Qiu[1], Xiyao Gu[3], Yongming Dai[4], Qun Xu[2], Yawen Sun[1], Yan Zhou[1]**

[1]Department of Radiology, Renji Hospital, School of Medicine, Shanghai Jiao Tong University, Shanghai, China; [2]Department of Neurology, Renji Hospital, School of Medicine, Shanghai Jiao Tong University, Shanghai, China; [3]Department of Anesthesiology, Renji Hospital, School of Medicine, Shanghai Jiao Tong University, Shanghai, China; [4]School of Biomedical Engineering, ShanghaiTech University, Shanghai, China

*Contributions:* (I) Conception and design: Y Zhou, Y Sun; (II) Administrative support: Y Zhou; (III) Provision of study materials or patients: Q Xu, Y Chen, Y Qiu; (IV) Collection and assembly of data: X Han, Y Wang; (V) Data analysis and interpretation: Y Dai, X Gu, X Han; (VI) Manuscript writing: All authors; (VII) Final approval of manuscript: All authors.

[#]These authors contributed equally to this work.

*Correspondence to:* Yawen Sun, MD, PhD; Yan Zhou, MD, PhD. Department of Radiology, Renji Hospital, School of Medicine, Shanghai Jiao Tong University, 160 Pujian Road, Pudong New Area, Shanghai 200127, China. Email: cjs1119@hotmail.com; clare1475@hotmail.com.

**Background:** White-matter hyperintensity (WMH) is the key magnetic resonance imaging (MRI) marker of cerebral small-vessel disease (CSVD). This study aimed to investigate whether habitat analysis based on physiologic MRI parameters can predict the progression of WMH and cognitive decline in CSVD.

**Methods:** Diffusion- and perfusion-weighted imaging data were obtained from 69 patients with CSVD at baseline and at 1-year of follow-up. The white-matter region was classified into constant WMH, growing WMH, shrinking WMH, and normal-appearing white matter (NAWM) according to the T2-fluid-attenuated inversion recovery (FLAIR) sequences images at the baseline and follow-up. We employed k-means clustering on a voxel-wise basis to delineate WMH habitats, integrating multiple diffusion metrics and cerebral blood flow (CBF) values derived from perfusion data. The WMH at the baseline and the predicted WMH from the habitat analysis were used as regions of avoidance (ROAs). The decreased rate of global efficiency for the whole brain structural connectivity was calculated after removal of the ROA. The association between the decreased rate of global efficiency and Montreal Cognitive Assessment (MoCA) and mini-mental state examination (MMSE) scores was evaluated using Pearson correlation coefficients.

**Results:** We found that the physiologic MRI habitats with lower fractional anisotropy and CBF values and higher mean diffusivity, axial diffusivity, and radial diffusivity values overlapped considerably with the new WMH (growing WMH of baseline) after a 1-year follow-up; the accuracy of distinguishing growing WMH from NAWM was 88.9%±12.7% at baseline. Similar results were also found for the prediction of shrinking WMH. Moreover, after the removal of the predicted WMH, a decreased rate of global efficiency had a significantly negative correlation with the MoCA and MMSE scores at follow-up.

**Conclusions:** This study revealed that a habitat analysis combining perfusion with diffusion parameters could predict the progression of WMH and related cognitive decline in patients with CSVD.

**Keywords:** Cerebral small-vessel disease (CSVD); white-matter hyperintensities (WMHs); habitat analysis; cognitive decline

Submitted Feb 04, 2024. Accepted for publication Jul 18, 2024. Published online Aug 28, 2024.
doi: 10.21037/qims-24-238
**View this article at:** https://dx.doi.org/10.21037/qims-24-238

## Introduction

Subcortical vascular cognitive impairment (SVCI), an important subtype of vascular cognitive impairment, is induced by cerebral small-vessel disease (CSVD) (1,2). SVCI progresses through two distinct phases: initially, it manifests as subcortical vascular mild cognitive impairment (svMCI) and is followed by the more advanced phase of vascular dementia (VaD). Over half of patients with svMCI eventually progress to VaD due to cognitive function deterioration (3). Effective strategies to combat this include early monitoring of vascular high-risk factors, dietary adjustments, and aerobic exercise, which can delay or even reverse the progression (4). Thus, early detection of cognitive function deterioration in patients with CSVD is crucial for timely intervention against VaD (5,6).

White-matter hyperintensities (WMHs), as crucial magnetic resonance imaging (MRI) markers, can indicate CSVD damage (7). These lesions can disrupt specific fiber tracts, impede effective communication within the white-matter network, and ultimately cause cognitive decline (8,9). Although previous studies have linked WMH burden and cognitive outcomes in patients with SVCI, this relationship has not been established in clinical practice (10-13). Simply monitoring total WMH volume changes over time may not fully capture its complex association with cognitive impairment, while solely focusing on aggregated WMH features can neglect intra-WMH heterogeneity. These insufficient approaches could obscure a comprehensive understanding of how WMH progression impacts cognitive function.

Although conventional MRI is capable of detecting WMH, novel imaging techniques can offer additional insights. Diffusion tensor imaging (DTI) can assess the tissue microstructure by measuring microscopic water movement, which is notably higher in WMH (11). DTI can characterize white-matter network disruption, a primary cause of cognitive impairment in SVCI, and detect subtle tissue alternations of the WMH penumbra (5,7,12). The WMH penumbra is an area of white matter surrounding the WMH but with normal signal on fluid-attenuated inversion recovery (FLAIR) images. Similarly, arterial spin labeling (ASL) can identify areas of hypoperfusion within the penumbra (11). WMHs and their associated penumbras constitute a spectrum of white-matter damage, as abnormal changes to normal-appearing white matter (NAWM) often precede WMH expansion. Although these imaging techniques can provide a degree of insight into WMH development, there is lack of understanding regarding the specific NAWM alternations that evolve into WMHs. Acquiring greater clarity in this area may elucidate the nature of the clinical variation observed in patients with CSVD.

By leveraging advanced postprocessing algorithms, habitat analysis of radiological imaging can define subregions within a heterogeneous tumor, identifying voxels with similar tumor features (14). This voxel-level analysis provides pathophysiological insights into WMH progression, revealing tissue microenvironment heterogeneity. It is compatible with various neuroimaging methods, including diffusion- and perfusion-weighted MRI (14). Given the dynamic nature of WMH and its associated penumbras, investigating their evolution through spatial and temporal heterogeneity, as well as cognition-related imaging biomarkers, holds pivotal clinical value (15). Employing diffusion and perfusion MRI for habitat analysis in those with CSVD could improve our understanding of WMH progression and cognitive impairment.

Various etiologies and cerebrovascular risk factors are associated with WMH, yet the related neuropathological mechanisms have not been elucidated. Understanding these mechanisms is crucial for the prognosis and early intervention in patients with CSVD (16). In this study, we aimed to determine whether habitat analysis using physiological MRI in combination with structural connectivity analysis could predict WMH progression and cognitive decline. We propose that a temporal and spatial habitat analysis based on DTI and ASL can facilitate the identification of NAWM regions prone to future WMH development. We present this article in accordance with the STROBE reporting checklist (available at https://qims.amegroups.com/article/view/10.21037/qims-24-238/rc).

 

## Methods

### *Participants*

This study was conducted in accordance with the Declaration of Helsinki (as revised in 2013) and was approved by the research ethics committee of Renji Hospital (approval no. RA2021-645). Written informed consent was obtained from all patients. Participants were recruited from the Stroke Clinic of Renji Hospital between April 2020 and July 2022, and most had experienced a clinical lacunar stroke at least 3 months before the study. Imaging assessment of each CSVD marker was rated by two well-trained radiologists (X.H. and Y.W.) according to the Standards for Reporting Vascular Changes on Neuroimaging (STRIVE) (17). Images with inconsistent results were ultimately assessed by another senior radiologist (YW Sun). All radiologists were blinded to the participants' clinical data.

The clinical data including sociodemographic, clinical information, patient history, and MRI data were collected for all participants. The exclusion criteria were as follows: (I) cerebral hemorrhages, cortical and/or subcortical nonlacunar territorial infarcts, and watershed infarcts; (II) identifiable causes of white-matter lesions (e.g., multiple sclerosis, sarcoidosis, and brain irradiation); (III) other neurodegenerative diseases, including Alzheimer and Parkinson diseases; (IV) signs of normal pressure hydrocephalus or alcoholic encephalopathy; (V) low education levels (<6 years); (VI) severe depression [Hamilton Depression Rating Scale (HDRS) ≥18], other psychiatric comorbidities, or severe cognitive impairment (inability to perform neuropsychological tests); (VII) severe claustrophobia and contraindications to MRI (e.g., pacemaker and metallic foreign bodies); and (VIII) poor image quality or missing of clinical data. Finally, 86 participants were included (7 were excluded: cerebral hemorrhages =2, low education levels =2, poor image quality =1, and missing clinical data =2).

### *Neuropsychological assessment*

The neuropsychological assessments of the participants were conducted by two seasoned neurologists at baseline and 1-year follow-up, timed to occur within 2 weeks before or after the completion of MRI procedures. None of participants experienced a new clinical stroke or transient ischemic attack in the interval between MRI procedures. The following extensive set of neuropsychological assessments were used: Trail-Making Test A and B, Stroop color-and-word test, verbal fluency (category) test, auditory verbal learning test (short and long delayed free recall), Rey-Osterrieth complex figure test-delayed recall), Boston Naming Test (30 words), Rey-Osterrieth complex figure test-copy, Lawton-Brody Instrumental Activities of Daily Living (ADL) scale test, Barthel Index (BI), HDRS, and the Neuropsychiatric Inventory.

To evaluate the participants' cognitive statuses, the scores for each measure of normal-aged individuals in Shanghai, China, were used as the normal baseline (norms) (18). Cognitive dysfunction was defined as a performance at least 1.5 standard deviations (SDs) below the mean on at least one neuropsychological test. As per the Statement on Vascular Contributions to Cognitive Impairment and Dementia of the American Heart Association (AHA) (19), VaD diagnosis requires a cognitive decline from a previous level and deficits in at least two cognitive domains sufficiently severe to interfere with daily functions without being influenced by the motor or sensory aftermath of the vascular event. The criteria for svMCI included the following: (I) normal or mildly impaired ADL; (II) no fulfilment of dementia criteria; and (III) detectable mild cognitive declines in domains such as attention, executive function, memory, language, and visuospatial skills. We assessed functional abilities using BI and Lawton-Brody ADL scales. Patients with disabilities from cognitive and motor sequelae were rigorously excluded based on their cognitive impairment history and clinical assessment. Non-cognitive impairment (NCI) denotes subcortical vascular disease absent of cognitive deficits, with all neuropsychological assessments within normal limits (>–1.5 SD) (18). Overall cognitive performance was gauged using the Montreal Cognitive Assessment (MoCA) and mini-mental state examination (MMSE) (20,21). The study initially categorized 86 participants into 33 with NCI, 36 with MCI, and 17 with VaD, yet only 69 participants (33 NCI and 36 MCI) were ultimately included.

### *MRI data and preprocessing*

MRI examinations were carried out at baseline and at 1-year follow-up on a 3.0-T MRI scanner (Signa HDxt; GE HealthCare, Chicago, IL, USA) equipped with an eight-channel phase array head coil, and two foam paddings were used to restrict head motion. Several MRI sequences were performed. (I) DTI was conducted under the following parameters: field of view (FOV) =256×256 mm, repetition

 

time (TR)/echo time (TE) =17,000/89.8 ms, slice thickness/gap =2.0/0 mm, number of slices =66, matrix size =128×128, diffusion-weighted directions =20, b-value =1,000 s/mm$^2$, and acquisition time =6 min 14 seconds). (II) ASL was performed based on a three-dimensional fast spin-echo (FSE) sequence, featuring a 1,500-ms labeling duration followed by a 2,000-ms delay after labeling. ASL acquisition included six averages: one proton density-weighted image and six pairs of labeled and unlabeled images. These were averaged to produce a single mean perfusion-weighted image (unlabeled-labeled) [FOV =240×240 mm, TR/TE =4,337/9.8 ms, slice thickness =4 mm, matrix size =128×128, flip angle =155°, number of excitations (NEX) =3, number of slices =34, scanning time = 4 min 12 seconds]. The cerebral blood flow (CBF) map was automatically calculated on the Signa HDxt MRI console, which was calculated according to the following equation:

$$\mathrm{CBF} = 6000 * \lambda \frac{\left(1-\exp\left(-\frac{\mathrm{ST(s)}}{\mathrm{T_{1t}(s)}}\right)\right)\exp\left(\frac{\mathrm{PLD(s)}}{\mathrm{T_{1b}(s)}}\right)}{2\mathrm{T_{1b}(s)}\left(1-\exp\left(-\frac{\mathrm{LT(s)}}{\mathrm{T_{1b}(s)}}\right)\right)\varepsilon * \mathrm{NEX_{PW}}}\left(\frac{\mathrm{PW}}{\mathrm{SF_{PW}PD}}\right) \quad [1]$$

where $T_{1b}$ is the T1 of blood and is assumed to be 1.6 s at 3.0T [the partial saturation of the reference image (proton density-weighted image) was corrected by using a $T_{1t}$ of 1.2 s (typical of gray matter)]; ST is the saturation time and is set to 2 s; the partition coefficient, λ, is set to the whole brain average, 0.9; the efficiency, ε, is a combination of both inversion efficiency (0.8) and background suppression efficiency (0.75) resulting in an overall efficiency of 0.6; PLD is the postlabeling delay used for the ASL experiment; LT is the labeling duration and is set to 1.5 s; and PW is the perfusion-weighted or the raw difference image. (III) Sagittal T1-weighted images encompassing the entire brain were obtained using the three-dimensional fast spoiled gradient recalled echo (SPGR) sequence under the following parameters: FOV =256×256 mm, TR/TE =5.6 /1.8 ms, TI =450 ms, slice thickness/gap =1.0/0 mm, number of slices =156, flip angle =15°, matrix size =256×256, acquisition time =3 min 53 seconds. (IV) T2-FLAIR sequences were conducted under the following parameters: FOV =256×256 mm, TR/TE =9,075/150 ms, TI =2,250 ms, matrix size =256×256, slice thickness =2 mm, number of slices =66, and acquisition time =7 min 18 s.

The DTI data were preprocessed with the FMRIB's Software Library. The major procedures involved skull removal, gap cropping, motion correction, eddy current distortion rectification, and diffusion tensor calculations. The derived maps of fractional anisotropy (FA), mean diffusivity (MD), axial diffusivity (AD), and radial diffusivity (RD), as well as the FLAIR images and normalized CBF maps, were each coregistered in native space with their corresponding T1-weighted images. The baseline T1-weighted images were automatically segmented into distinct categories, namely WM, gray matter, cerebrospinal fluid, and other regions. This segmentation was accomplished using the SPM toolbox in MATLAB (MathWorks, Natick, MA, USA).

### *Automatic WMH segmentation and habitat analysis*

The automatic segmentation of WMH was conducted based on the methodologies presented in a previous study (22). The WMH mask was also used to correct the entire white-matter region. After the linear coregistration of the baseline and follow-up T1-weighted and FLAIR images, the entire white-matter region of the baseline was divided into four distinct subregions (*Figure 1*). We subsequently found that the FLAIR images had thicker slices (2 mm) compared to the T1 images (1 mm). To avoid registration errors due to this discrepancy, we interpolated the FLAIR images to match the slice thickness of the T1-weighted images. This process minimized the potential for mismatch and ensured more accurate coregistration. We used a method that involved interpolating the images to ensure consistency in voxel size and followed this by applying coregistration and subtraction techniques to identify changes.

The entire white-matter region of the baseline was segmented into four parts, including NAWM (areas not showing WMH at either baseline or follow-up), constant WMH (areas showing WMH at both baseline and during follow-up), growing WMH (areas without WMH at baseline but with WMH during follow-up), and shrinking WMH (areas showing WMH at baseline but not during follow-up). This method of partitioning the entire white-matter region according to the baseline and follow-up FLAIR images was used as the gold standard for the subsequent prediction that only used the baseline physiologic parameters from DTI and ASL data.

We performed habitat analysis, an unsupervised clustering method, based on the parametric maps of FA, MD, AD, RD, and CBF at the baseline. The procedure included the following steps:

(I) Normalization: for each participant, the five parameters (FA, MD, AD, RD, and CBF) were all

 

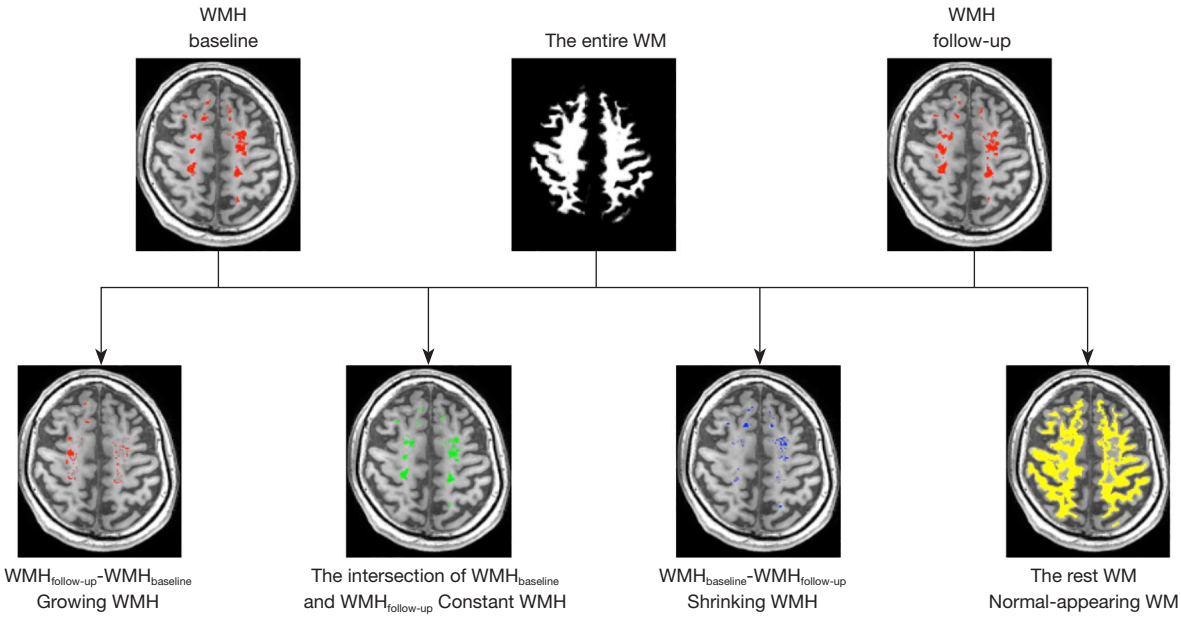


**Figure 1** The entire white matter was divided into four distinct subregions according to the FLAIR images at baseline and follow-up. These included growing WMH (areas without WMH at baseline but with WMH during follow-up), constant WMH (areas showing WMH at both baseline and follow-up), shrinking WMH (areas showing WMH at baseline but not during the follow-up), and normal-appearing WM (the remaining white-matter areas). WM, white matter; WMH, white-matter hyperintensity; FLAIR, fluid-attenuated inversion recovery.

standardized using z-score.

(II) Clustering: we employed the script of k-means in MATLAB, with the number of clusters being k=2 or 3, distance parameters set to "city block", 100 replications, and with other parameters set to their default values. To distinguish between growing WMH and NAWM, we used a habitat analysis strategy in which all the non-WMH voxels at the baseline were clustered according to their similarities using the L1 distances between the voxel intensities and similarity metric. All clusters were displayed as spatial habitats in the original image space, using the k-means clustering algorithm.

(III) Evaluation: the performance of habitat analysis in predicting growing WMH was evaluated by calculating the volumes of overlapping regions between the physiologic habitats and growing WMH, as well as metrics including accuracy, sensitivity, and specificity.

Similarly, we conducted habitat analysis on all the WMH voxels at the baseline to differentiate shrinking WMH from constant WMH for each participant. We chose the optimum number of clusters when obtaining the best performance to ensure the results were explainable. The flowchart of habitat analysis is provided in *Figure 2*.

### *Effect of WMH on the structural network*

To evaluate the effect of the WMH during the baseline and the predicted WMH from the habitat analysis on the structural connectome, the WMH regions during the baseline and follow-up were used as regions of avoidance (ROAs) in DTI tractography for each patient, respectively. The structural connectivity was calculated using DSI studio (http://dsi-studio.labsolver.org/) with q-space diffeomorphic reconstruction (QSDR) and whole-brain fiber tracking with $10^7$ seed points and the fiber length set from 20 to 400 mm. The Brainnectome parcellation map was used to define connectivity nodes, and the density-weighted structural connectivity matrix was calculated with a sparsity of 0.9. The decreased rate of global efficiency was estimated on the basis of the whole brain connectivity matrices with and without ROAs.

### *Statistical analysis*

All statistical analysis was performed in MATLAB. To

 

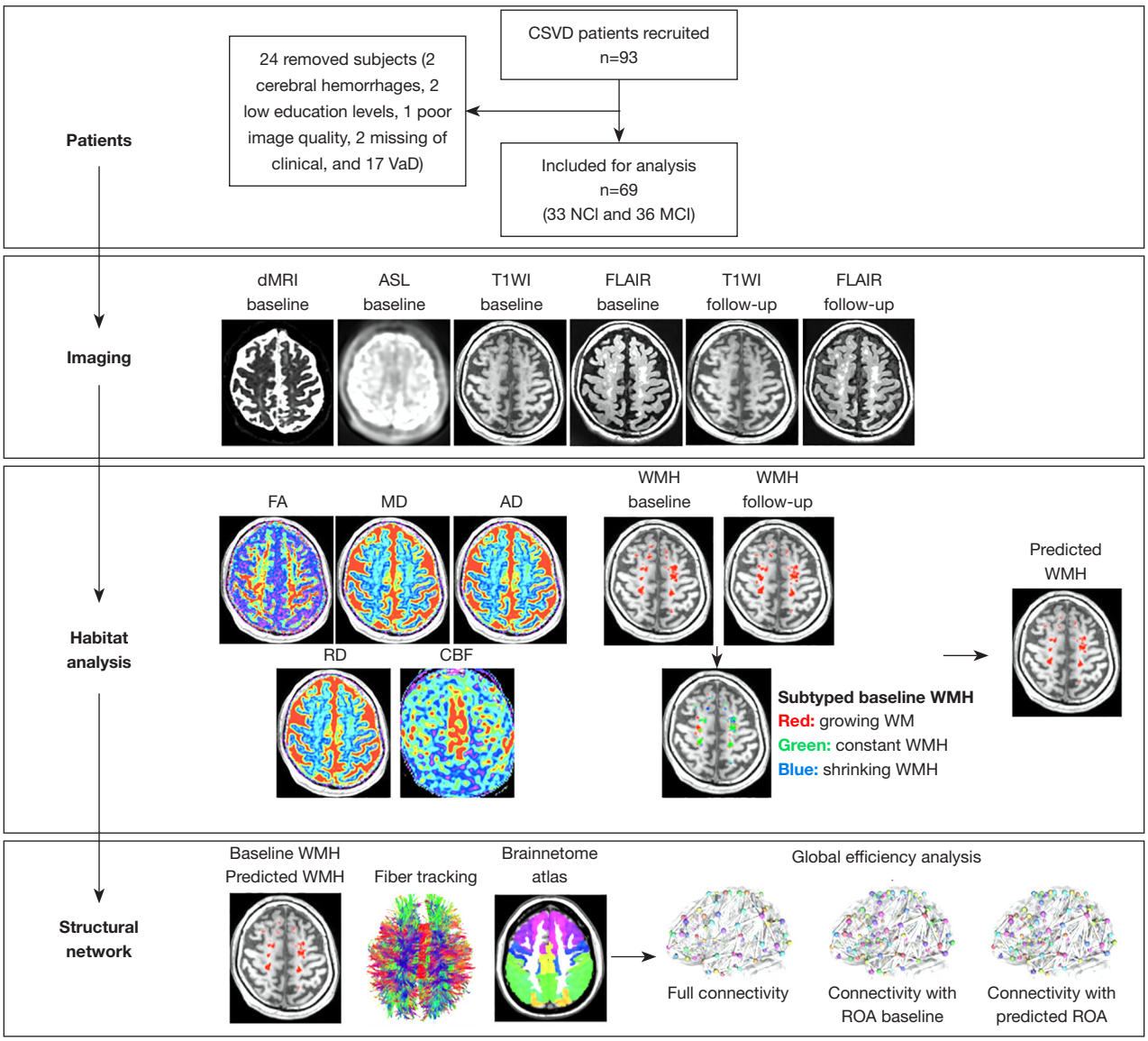


**Figure 2** The flowchart of the study procedure. VaD, vascular dementia; CSVD, cerebral small-vessel disease; NCI, non-cognitive impairment; MCI, mild cognitive impairment; dMRI, diffusion magnetic resonance imaging; ASL, arterial spin labeling; T1WI, T1-weighted image; FLAIR, fluid-attenuated inversion recovery image; FA, fractional anisotropy; MD, mean diffusivity; AD, axial diffusivity; WMH, white-matter hyperintensity; RD, radial diffusivity; CBF, cerebral blood flow; ROA, region of avoidance.

identify physiological differences between the NAWM and growing WMH regions and between the constant WMH and shrinking WMH regions, diffusion and perfusion parameters (FA, MD, AD, RD, and CBF) were calculated via a two-tailed Wilcoxon matched-pairs signed-rank test. Moreover, we conducted two-samples *t* tests on the decreased rate of global efficiency between the MCI and NC groups, and Pearson correlation analysis between the decreased rate of global efficiency and the scores of the MMSE/MoCA. Subsequently, a power analysis was conducted using MATLAB scripts (MathWorks), with the sampsizepwr and binofit functions being used to calculate the power for the sample size in this study. The power analysis was based on determining significant associations between imaging parameters and cognition. A P value <0.05 was considered statistically significant.

**Table 1** The demographic and clinical outcome of all patients with CSVD

| Clinical outcome | CSVD patients (n=69) | | P value |
|---|---|---|---|
| | Baseline | One-year follow-up | |
| Age (years) (mean ± SD) | 66.2±6.7 | 66.2±6.7 | NA |
| Gender (No.) | | | NA |
| Male | 54 | 54 | |
| Female | 15 | 15 | |
| Cognitive subtype (No.) | | | >0.99 |
| MCI | 36 | 36 | |
| NC | 33 | 33 | |
| MMSE (mean ± SD) | 27.7±2.0 | 27.7±2.0 | 0.93 |
| MoCA (mean ± SD) | 23.5±3.7 | 23.4±3.5 | 0.79 |

CSVD, cerebral small-vessel disease; SD, standard deviation; NA, not applicable; MCI, mild cognitive impairment; NC, normal cognition; MMSE, mini-mental state examination; MoCA, Montreal Cognitive Assessment.

## Results

A total of 69 participants with CSVD were enrolled in this study, which included a baseline evaluation and 1-year follow-up. The demographic characteristics and clinical outcomes of all participants are listed in *Table 1*. There were no significant differences in MMSE or MoCA scores from the baseline to the 1-year follow-up (both P values >0.5). All participants were categorized into an MCI or NC group, and there were no significant differences in gender or age between these two groups (both P values >0.05, *Table 1*).

Before habitat analysis was performed, five physiologic parameters (FA, MD, AD, RD, and CBF) were calculated between growing WMH and NAWM, all of which showed significant differences between the two groups (sum of signed ranks: FA: −2,004; MD: 2,346; AD: 2,346; RD: 2,342; CBF: −2,278; *Figure 3*). These five parameters were compared between shrinking WMH and constant WMH at baseline and also showed significant differences (sum

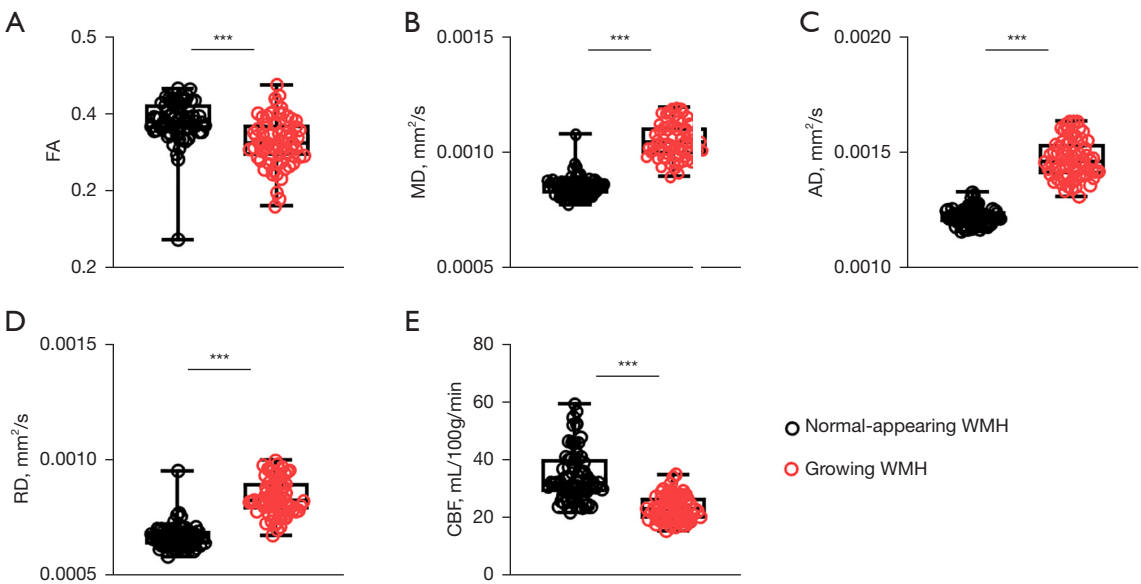


**Figure 3** The comparisons of physiological parameters between normal-appearing white matter and growing WMH. The physiological parameters including (A) FA, (B) MD, (C) AD, (D) RD, and (E) CBF showed significant differences between normal-appearing white matter and growing WMH regions according to a two-tailed Wilcoxon matched-pairs signed-rank test. Sum of signed ranks: FA: −2,004; MD: 2,346; AD: 2,346; RD: 2,342; CBF: −2,278. ***, P<0.001. FA, fractional anisotropy; MD, mean diffusivity; AD, axial diffusivity; RD, radial diffusivity; CBF, cerebral blood flow; WMH, white-matter hyperintensity.

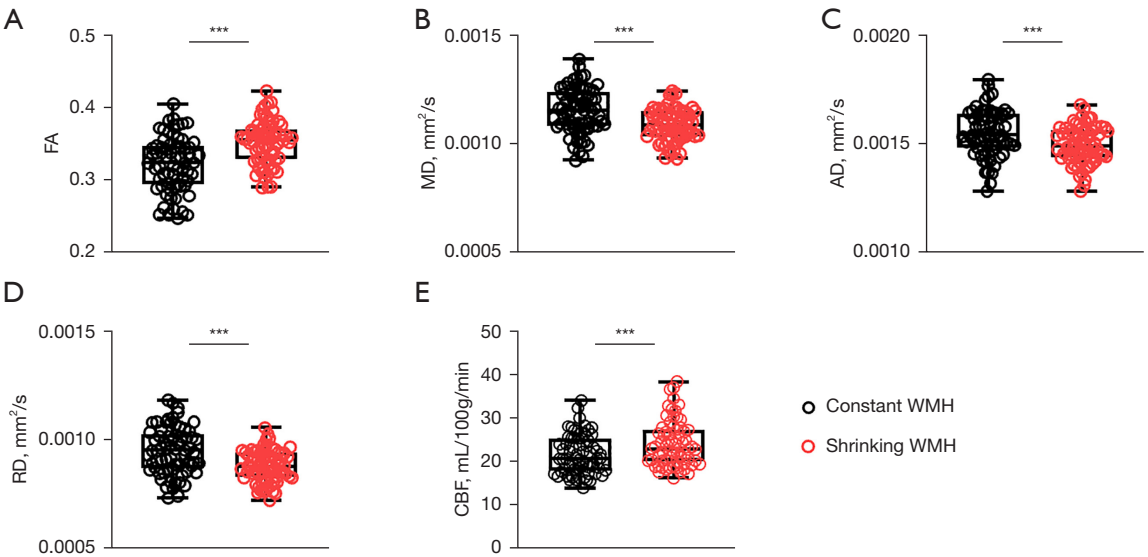


**Figure 4** The comparisons of physiological parameters between constant and shrinking WMH. The physiological parameters including (A) FA, (B) MD, (C) AD, (D) RD, and (E) CBF showed significant differences between constant and shrinking WMH regions according to a two-tailed Wilcoxon matched-pairs signed-rank test. Sum of signed ranks: FA: 2,014; MD: −2,074; AD: −1,742; RD: −2,100; CBF: 2,084. ***, P<0.001. FA, fractional anisotropy; MD, mean diffusivity; AD, axial diffusivity; RD, radial diffusivity; CBF, cerebral blood flow; WMH, white-matter hyperintensity.

**Table 2** The performance of habitat analysis in predicting growing WMH and shrinking WMH

| Number of clusters | Accuracy (%) | Sensitivity (%) | Specificity (%) |
|---|---|---|---|
| Predicting growing WMH | | | |
| k=2 | 88.9±12.7 | 91.4±13.5 | 86.5±12.3 |
| k=3 | 71.1±8.9 | 80.2±10.4 | 65.0±7.7 |
| Predicting shrinking WMH | | | |
| k=2 | 76.6±12.3 | 79.8±12.6 | 75.4±11.0 |
| k=3 | 65.9±9.3 | 70.3±10.5 | 61.5±8.7 |

Data are represented as mean ± standard deviation. WMH, white-matter hyperintensity.

of signed ranks: FA: 2014; MD: −2,074; AD: −1,742; RD: −2,100; CBF: 2,084; *Figure 4*).

According to these imaging distinctions, habitat analysis was performed to discriminate between growing WM and NAWM and between shrinking WMH and constant WMH. With the number of clusters set to two (k=2), the accuracy for differentiating growing WMH from NAWM using the physiological MRI habitat with lower FA and CBF values and higher MD, AD, and RD values was 88.9%±12.7%. The sensitivity and specificity for this differentiation were 91.4%±13.5% and 86.5%±12.3%, respectively (*Table 2*). When the number of clusters was increased to three (k=3), the corresponding accuracy was reduced to 71.1%±8.9%, and the sensitivity and specificity were 80.2%±10.4% and 65.0%±7.7%, respectively (*Table 2*). Similarly, the physiological MRI habitat with higher FA and CBF values and lower MD, AD, and RD values achieved accuracies of 76.6%±12.3% and 65.9%±9.3% in distinguishing shrinking WMH from constant WMH, when the number of clusters was set to two and three, respectively (*Table 2*). However, neither the volume of growing WMH and shrinking WMH nor the physiologic parameters within these regions showed any significant correlation with cognitive scale scores (all P values >0.05). These data indicated that habitat analysis could characterize WMH heterogeneity and predict growing WMH with a relatively high accuracy and specificity. A growing WMH was typically associated with lower FA and CBF values and with higher MD, AD, and RD values.

To further test the efficacy of habitat analysis, we assessed the impact of WMH, both at baseline and as predicted from habitat analysis, on structural connectome. The WMH regions identified at baseline and predicted for the follow-

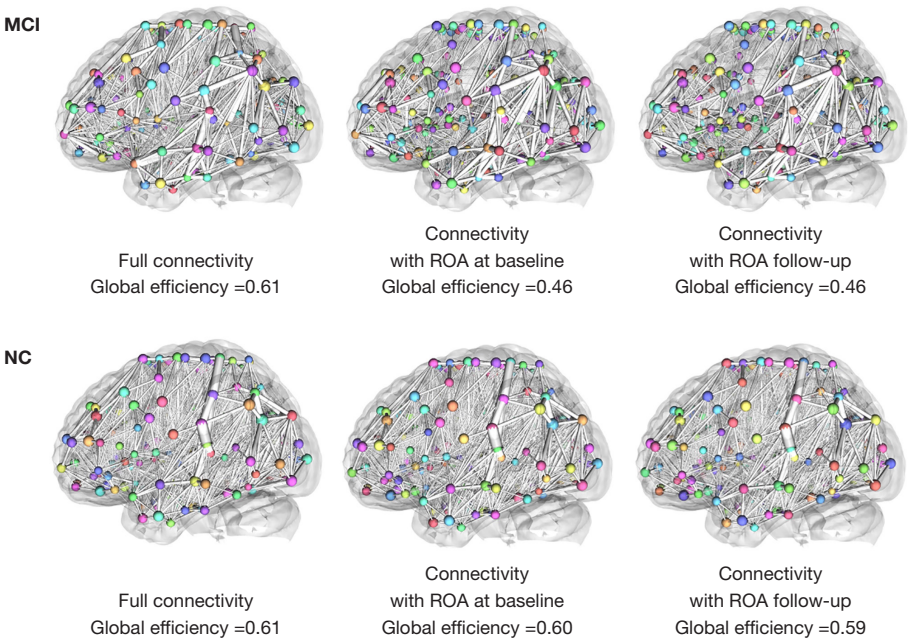


**Figure 5** The structural connectivity network in representative MCI and NC patients. We estimated the full connectivity, the connectivity with the WMH region during baseline as the ROA, and the connectivity with the predicted WMH region (using habitat analysis) as the ROA and calculated the corresponding global efficiency. MCI, mild cognitive impairment; ROA, region of avoidance; NC, normal cognition; WMH, white-matter hyperintensity.

up period were integrated as ROAs in DTI tractography for each patient. *Figure 5* shows an example of the white-matter structural connectivity network with and without the consideration of the WMH region as the ROA in representative MCI and NC patients. After the removal of the WMH region, we observed a significant decrease in the global efficiency of the white-matter network. Interestingly, the percentage decrease significantly diverged between the MCI and the NC groups at baseline and follow-up (baseline: t=2.774; follow-up: t=2.348; *Figure 6A*,*6B*). Moreover, the percentage decrease exhibited a negative correlation with the cognitive scale scores (MMSE: r=−0.39, P=0.003; MoCA: r=−0.41, P=0.002; *Figure 6C*). Upon further analysis, when the predicted WMH was removed, the global efficiency of the white-matter network declined during the follow-up period. Once again, the percentage decrease was negatively correlated with the cognitive scale scores (MMSE: r=−0.36; P=0.01; MoCA: r=−0.38; P=0.006; *Figure 6D*).

Given our sample size consisting of 36 participants with MCI and 33 participants with normal cognition, the statistical powers associated with the significant differences in the percentage decrease of global efficiency of MCI and NC groups and their consequential correlations with the cognitive scale scores exceeded 0.80. This implies a strong probability of correctly rejecting the null hypothesis, thereby affirming the robustness of our findings.

## Discussion

In this study, we compiled an extensive and diverse dataset including both clinical and neuropsychological assessments complemented by multimodal MRI data from the cohort diagnosed with CSVD who were followed up for a duration of 1 year. Our analysis revealed that habitat analysis, based on baseline perfusion- and diffusion-weighted images, could characterize WMH heterogeneity and predict growing WMH and the related cognitive decline. Notably, the prognostic utility of the habitat analysis was found to surpass traditional clinical scales. The primary finding of this study was that habitat analysis could effectively discriminate between growing WMH and NAWM and between shrinking and constant WMH. Growing WMH was associated with relatively lower FA and CBF values and higher MD, AD, and RD values, an observation of critical importance for understanding the clinical implications of the results. The efficacy of the WM

 

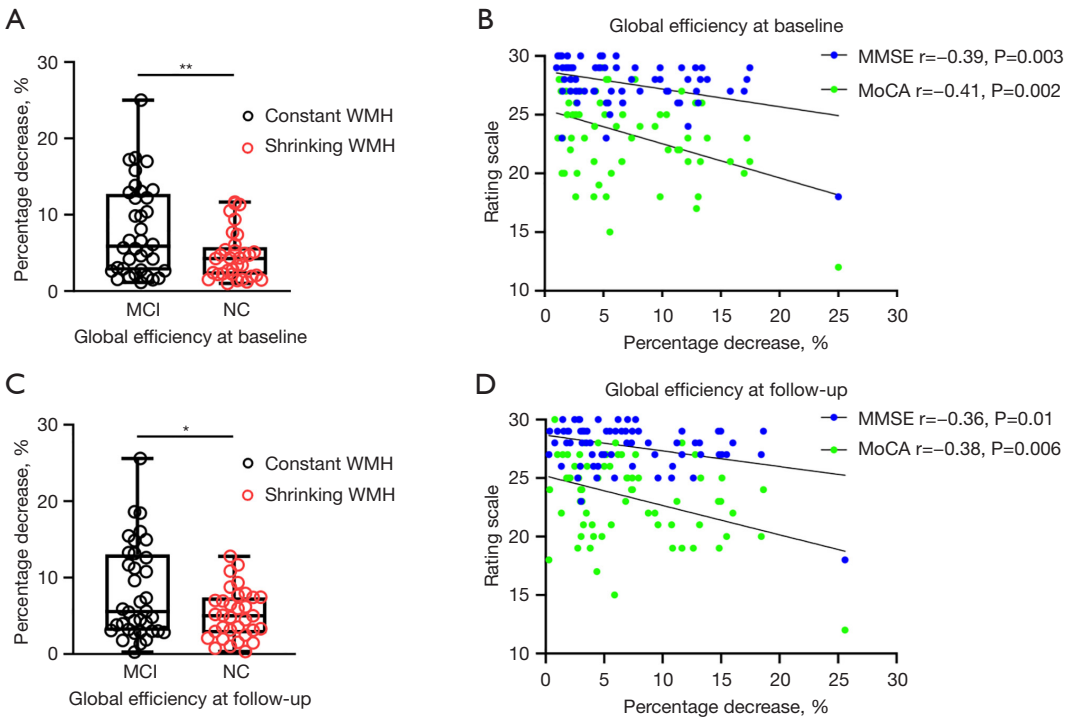


**Figure 6** The comparisons of global efficiency decrease between MCI and NC patients and its relationship with cognitive rating scales. (A,B) The percentage decrease in global efficiency showed significant differences between the MCI and NC patients during baseline and follow-up [(A) baseline: t=2.774; (B) follow-up: t=2.348]. (C,D) The percentage decrease in global efficiency were negatively correlated with the MMSE and MoCA scores in all patients at baseline [(C) MMSE: r=−0.39, P=0.003; MoCA: r=−0.41, P=0.002] and follow-up [(D) MMSE, r=−0.36, P=0.01; MoCA, r=−0.38, P=0.006]. *, P<0.05; **, P<0.01. MCI, mild cognitive impairment; NC, normal cognition; WMH, white-matter hyperintensity; MMSE, mini-mental state examination; MoCA, Montreal Cognitive Assessment.

network declined considerably when the predicted WMH region was excluded. Additionally, a negative correlation was found between the percentage decrease and cognitive scale scores. In summary, our findings suggest that the application of imaging-based habitat analysis could provide complementary prognostic information.

WMH damages white-matter fibers, impairs cognition, and increases the risk of dementia (11,23,24), with 80% of new WMH lesions extending from existing ones (7). Prior research indicates that the penumbras around WMH, marked by DTI metrics, typically extend from 2 to 9 mm in extent. In contrast, blood flow in the brain, as determined by ASL, generally spans about 12 to 14 mm (25-28). This suggests that CBF penumbras are more extensive than are the structural changes in surrounding NAWM. WMH progression, marked by low perfusion and white-matter integrity loss, involves accumulating small vessels, demyelination, and axonal injury, which manifest as changing ASL and DTI parameters. This damage transforms NAWM into WMH, with cascading effects. WMH heterogeneity complicates imaging studies, making sole WMH analysis insufficient for an understanding of its progression (13). Our study found significant differences in all five physiologic parameters of FA, MD, AD, RD, and CBF between growing WMH and NAWM and between shrinking WMH and constant WMH, providing a basis for predicting WMH changes through habitat analysis. Besides, we found shrinking WMH to be significant, challenging prior attributions to technical issues such as segmentation and registration and underscoring its importance in future research. This highlights potential positive implications for patients with CSVD.

In our habitat analysis, we found that baseline MRI habitats with lower FA and CBF values but higher MD, AD, and RD value overlapped considerably with new WMH at the follow-up. This finding suggests that visible WMH progression on conventional FLAIR imaging is a superficial finding indicative of a much deeper issue. The underlying

loss of microstructural integrity and low perfusion are detectable only using advanced neuroimaging techniques. Our results indicate that long-term hypoperfusion is the earliest pathological change in cerebrovascular disease, leading to WM microstructural lesions and eventually visible WMH on FLAIR. Growing WMH could be influenced by a hypoxic microenvironment.

FA, MD, AD, and RD reflect white-matter integrity. MD correlates with broad cognitive impairment, while FA only significantly correlates with visual space. Compared with MD, the correlation between FA and cognitive function is weaker, highlighting the internal heterogeneity of WMH, with FA and MD jointly affecting the cognitive function. Moreover, AD reflects the diffusivity of the main diffusion direction, which is a sign of axon damage, while RD is the diffusivity perpendicular to the main direction, which reflects the degree of demyelination. Previous studies have shown that AD and RD correlate differently with cognitive domains, which can explain the clinical variations in participants with a similar WMH burden (29,30). For instance, participants with degraded WMH microstructural integrity might experience more severe clinical symptoms than those with equivalent WMH extent but better microstructural integrity (4,7). This aligns with CSVD studies in which patients with substantial loss of microstructural integrity within their WMH had decreased cognitive performance regardless of WMH volume (29,31). The habitat of lower FA and CBF values and higher MD, AD, and RD values could potentially serve as a biomarker for WMH progression, providing a personalized foundation for individual intervention strategies (32).

Previous research has indicated that white matter microstructural damage disrupts cortico-subcortical pathways, thereby impairing brain network connectivity and reducing overall brain network transmission efficiency (33). A holistic approach to the brain is more effective in identifying imaging markers related to cognition. A brain network, with both the brain structure and function being mapped, focuses on the integration of information from structural damage across the whole brain (9). Numerous methods have been developed to study cognitive dysfunction through the construction of a brain network (34). CSVD damages white-matter fiber bundles, disrupting the complex network connecting the cortex and subcortical regions and altering cognitive function in SVCI. Network disruption reflects global structural and cognitive damage (35).

We observed a significant global efficiency decrease upon WMH removal, with notable differences between the MCI and NC groups. This reduction correlated negatively with cognitive function. In addition, treating baseline-predicted WMH as lesions revealed a similar decrease in network efficiency and its cognitive correlation. A longitudinal 5-year study produced evidence supporting the key role of structural network disruption in cognitive decline (36) and in line with our findings, found that individual lesions were not independently associated with cognition. It is likely that various pathological processes resulting in demyelination and reduction in axonal number and density may directly or indirectly impact the integrity of white-matter tracts (37,38). The structural brain network, representing the integrity of WM connectivity, offers comprehensive insights into cognitive dysfunction mechanisms.

Cognitive function relies on the interconnection and integration of multiple cortical regions. Thus individual focal lesions may not accurately reflect the functional disturbance at the core of cognitive decline. The greater sensitivity of brain network measures stems from their continuous, quantitative properties, which are highly sensitive to subtle disruptions in the microstructures (39). These results provide critical insights into the network properties of brain structural damage and cognitive impairment in patients with SVCI. CSVD's insidious nature, characterized by minor stroke(s) leading to gradual cognitive impairment, necessitates the use of surrogate neuroimaging marker to assess and monitor cognitive status. The network measures exhibited a correlation with cognitive impairment and could potentially serve as an indicator of cognitive decline. The WMH-induced disruption of brain networks is a critical process in the cognitive dysfunction in patients with CSVD.

Our study has a few potential limitations that should be mentioned. First, the 1-year follow-up period might not have been sufficiently long to observe a substantial cognitive decline in patients with CSVD compared to baseline measurements. Second, our habitat analysis was conducted on a patient-by-patient basis using individual MR images, which might have introduced variability due to the absence of unified segmentation criteria across all patients. The importance of individual MRI parameters was only cursorily evaluated in the k-means clustering model for habitat analysis. Third, the partial volume effect and slight misregistration can impact the definition of the four white-matter regions. Finally, our evaluation focused exclusively on the relationship between cognitive impairment and WMH concerning the global efficiency decrease of

 

the white-matter network. We did not delve into the contributions of specific subnetworks and subregions to the observed cognitive anomalies.

## Conclusions

WMH consists of multiple spatially distinct subregions. Through the integration of perfusion and diffusion parameters, habitat analysis could potentially predict progressive WMH and cognitive decline in those with CSVD.

## Acknowledgments

*Funding:* This work was supported by Medical Engineering Cross Research Foundation of Shanghai Jiao Tong University (No. YG2022QN035), the National Natural Science Foundation of China (No. 82171885), the Shanghai Science and Technology Committee Project (Explorer Project Funding No. 21TS1400700), the Shanghai Leading Talent Program of Shanghai Municipal Health Commission (No. 2022LJ023), and the Technology Standardized Management and Promotion Projects of Shanghai Shenkang Hospital Development Center (No. SHDC22023022).

## Footnote

*Reporting Checklist:* The authors have completed the STROBE reporting checklist. Available at https://qims.amegroups.com/article/view/10.21037/qims-24-238/rc

*Conflicts of Interest:* All authors have completed the ICMJE uniform disclosure form (available at https://qims.amegroups.com/article/view/10.21037/qims-24-238/coif). The authors have no conflicts of interest to declare.

*Ethical Statement:* The authors are accountable for all aspects of the work in ensuring that questions related to the accuracy or integrity of any part of the work are appropriately investigated and resolved. The study was conducted in accordance with the Declaration of Helsinki (as revised in 2013). The study was approved by the research ethics committee of Renji hospital (RA2021-645), and written informed consent was obtained from all patients.



## References

1. Uwagbai O, Kalish VB. Vascular Dementia. StatPearls. Treasure Island (FL), 2022.
2. Yin X, Han Y, Cao X, Zeng Y, Tang Y, Ding D, Zhang J. Association of deep medullary veins with the neuroimaging burden of cerebral small vessel disease. Quant Imaging Med Surg 2023;13:27-36.
3. Rossini PM, Miraglia F, Vecchio F. Early dementia diagnosis, MCI-to-dementia risk prediction, and the role of machine learning methods for feature extraction from integrated biomarkers, in particular for EEG signal analysis. Alzheimers Dement 2022;18:2699-706.
4. Alber J, Alladi S, Bae HJ, Barton DA, Beckett LA, Bell JM, et al. White matter hyperintensities in vascular contributions to cognitive impairment and dementia (VCID): Knowledge gaps and opportunities. Alzheimers Dement (N Y) 2019;5:107-17.
5. Han X, Zhang J, Chen S, Yu W, Zhou Y, Gu X. Mapping the current trends and hotspots of vascular cognitive impairment from 2000-2021: A bibliometric analysis. CNS Neurosci Ther 2023;29:771-82.
6. Han H, Ning Z, Yang D, Yu M, Qiao H, Chen S, Chen Z, Li D, Zhang R, Liu G, Zhao X. Associations between cerebral blood flow and progression of white matter hyperintensity in community-dwelling adults: a longitudinal cohort study. Quant Imaging Med Surg 2022;12:4151-65.
7. Jiaerken Y, Luo X, Yu X, Huang P, Xu X, Zhang M; Alzheimer's Disease Neuroimaging Initiative (ADNI). Microstructural and metabolic changes in the longitudinal progression of white matter hyperintensities. J Cereb Blood Flow Metab 2019;39:1613-22.
8. Tuladhar AM, Tay J, van Leijsen E, Lawrence AJ, van Uden IWM, Bergkamp M, van der Holst E, Kessels RPC, Norris D, Markus HS, De Leeuw FE. Structural network changes in cerebral small vessel disease. J Neurol Neurosurg Psychiatry 2020;91:196-203.
9. Lope-Piedrafita S. Diffusion Tensor Imaging (DTI). Methods Mol Biol 2018;1718:103-16.

 

10. Lin J, Wang D, Lan L, Fan Y. Multiple Factors Involved in the Pathogenesis of White Matter Lesions. Biomed Res Int 2017;2017:9372050.
11. van den Brink H, Doubal FN, Duering M. Advanced MRI in cerebral small vessel disease. Int J Stroke 2023;18:28-35.
12. Du J, Wang Y, Zhi N, Geng J, Cao W, Yu L, Mi J, Zhou Y, Xu Q, Wen W, Sachdev P. Structural brain network measures are superior to vascular burden scores in predicting early cognitive impairment in post stroke patients with small vessel disease. Neuroimage Clin 2019;22:101712.
13. Hu HY, Ou YN, Shen XN, Qu Y, Ma YH, Wang ZT, Dong Q, Tan L, Yu JT. White matter hyperintensities and risks of cognitive impairment and dementia: A systematic review and meta-analysis of 36 prospective studies. Neurosci Biobehav Rev 2021;120:16-27.
14. Lee DH, Park JE, Kim N, Park SY, Kim YH, Cho YH, Kim JH, Kim HS. Tumor Habitat Analysis Using Longitudinal Physiological MRI to Predict Tumor Recurrence After Stereotactic Radiosurgery for Brain Metastasis. Korean J Radiol 2023;24:235-46.
15. Lawrence AJ, Chung AW, Morris RG, Markus HS, Barrick TR. Structural network efficiency is associated with cognitive impairment in small-vessel disease. Neurology 2014;83:304-11.
16. Heng LC, Lim SH, Foo H, Kandiah N. Confluent White Matter in Progression to Alzheimer Dementia. Alzheimer Dis Assoc Disord 2021;35:8-13.
17. Duering M, Biessels GJ, Brodtmann A, Chen C, Cordonnier C, de Leeuw FE, et al. Neuroimaging standards for research into small vessel disease-advances since 2013. Lancet Neurol 2023;22:602-18.
18. Wu X, Ge X, Du J, Wang Y, Sun Y, Han X, Ding W, Cao M, Xu Q, Zhou Y. Characterizing the Penumbras of White Matter Hyperintensities and Their Associations With Cognitive Function in Patients With Subcortical Vascular Mild Cognitive Impairment. Front Neurol 2019;10:348.
19. Gorelick PB, Scuteri A, Black SE, Decarli C, Greenberg SM, Iadecola C, et al. Vascular contributions to cognitive impairment and dementia: a statement for healthcare professionals from the american heart association/american stroke association. Stroke 2011;42:2672-713.
20. Pendlebury ST, Markwick A, de Jager CA, Zamboni G, Wilcock GK, Rothwell PM. Differences in cognitive profile between TIA, stroke and elderly memory research sub-jects: a comparison of the MMSE and MoCA. Cerebrovasc Dis 2012;34:48-54.
21. Cockrell JR, Folstein MF. Mini-Mental State Examination (MMSE). Psychopharmacol Bull 1988;24:689-92.
22. Zhu W, Huang H, Zhou Y, Shi F, Shen H, Chen R, Hua R, Wang W, Xu S, Luo X. Automatic segmentation of white matter hyperintensities in routine clinical brain MRI by 2D VB-Net: A large-scale study. Front Aging Neurosci 2022;14:915009.
23. Debette S, Schilling S, Duperron MG, Larsson SC, Markus HS. Clinical Significance of Magnetic Resonance Imaging Markers of Vascular Brain Injury: A Systematic Review and Meta-analysis. JAMA Neurol 2019;76:81-94.
24. Wardlaw JM, Smith C, Dichgans M. Small vessel disease: mechanisms and clinical implications. Lancet Neurol 2019;18:684-96.
25. Maillard P, Fletcher E, Lockhart SN, Roach AE, Reed B, Mungas D, DeCarli C, Carmichael OT. White matter hyperintensities and their penumbra lie along a continuum of injury in the aging brain. Stroke 2014;45:1721-6.
26. Promjunyakul NO, Lahna DL, Kaye JA, Dodge HH, Erten-Lyons D, Rooney WD, Silbert LC. Comparison of cerebral blood flow and structural penumbras in relation to white matter hyperintensities: A multi-modal magnetic resonance imaging study. J Cereb Blood Flow Metab 2016;36:1528-36.
27. Promjunyakul N, Lahna D, Kaye JA, Dodge HH, Erten-Lyons D, Rooney WD, Silbert LC. Characterizing the white matter hyperintensity penumbra with cerebral blood flow measures. Neuroimage Clin 2015;8:224-9.
28. Maillard P, Fletcher E, Harvey D, Carmichael O, Reed B, Mungas D, DeCarli C. White matter hyperintensity penumbra. Stroke 2011;42:1917-22.
29. van Norden AG, de Laat KF, van Dijk EJ, van Uden IW, van Oudheusden LJ, Gons RA, Norris DG, Zwiers MP, de Leeuw FE. Diffusion tensor imaging and cognition in cerebral small vessel disease: the RUN DMC study. Biochim Biophys Acta 2012;1822:401-7.
30. Egle M, Hilal S, Tuladhar AM, Pirpamer L, Hofer E, Duering M, Wason J, Morris RG, Dichgans M, Schmidt R, Tozer D, Chen C, de Leeuw FE, Markus HS. Prediction of dementia using diffusion tensor MRI measures: the OPTIMAL collaboration. J Neurol Neurosurg Psychiatry 2022;93:14-23.
31. de Laat KF, van Norden AG, van Oudheusden LJ, van Uden IW, Norris DG, Zwiers MP, de Leeuw FE. Diffusion tensor imaging and mild parkinsonian signs in cerebral small vessel disease. Neurobiol Aging 2012;33:2106-12.
32. Li X, Yuan J, Qin W, Yang L, Yang S, Li Y, Hu W. Higher Total Cerebral Small Vessel Disease Burden Was Associated With Mild Cognitive Impairment and

 

Overall Cognitive Dysfunction: A Propensity Score-Matched Case-Control Study. Front Aging Neurosci 2021;13:695732.
33. Jokinen H, Koikkalainen J, Laakso HM, Melkas S, Nieminen T, Brander A, et al. Global Burden of Small Vessel Disease-Related Brain Changes on MRI Predicts Cognitive and Functional Decline. Stroke 2020;51:170-8.
34. Yuan JL, Wang SK, Guo XJ, Teng LL, Jiang H, Gu H, Hu WL. Disconnections of Cortico-Subcortical Pathways Related to Cognitive Impairment in Patients with Leukoaraiosis: A Preliminary Diffusion Tensor Imaging Study. Eur Neurol 2017;78:41-7.
35. Tuladhar AM, van Dijk E, Zwiers MP, van Norden AG, de Laat KF, Shumskaya E, Norris DG, de Leeuw FE. Structural network connectivity and cognition in cerebral small vessel disease. Hum Brain Mapp 2016;37:300-10.
36. Tuladhar AM, van Uden IW, Rutten-Jacobs LC, Lawrence A, van der Holst H, van Norden A, de Laat K, van Dijk E, Claassen JA, Kessels RP, Markus HS, Norris DG, de Leeuw FE. Structural network efficiency predicts conversion to dementia. Neurology 2016;86:1112-9.
37. Thomalla G, Glauche V, Koch MA, Beaulieu C, Weiller C, Röther J. Diffusion tensor imaging detects early Wallerian degeneration of the pyramidal tract after ischemic stroke. Neuroimage 2004;22:1767-74.
38. de Laat KF, Tuladhar AM, van Norden AG, Norris DG, Zwiers MP, de Leeuw FE. Loss of white matter integrity is associated with gait disorders in cerebral small vessel disease. Brain 2011;134:73-83.
39. Smith EE, Beaudin AE. New insights into cerebral small vessel disease and vascular cognitive impairment from MRI. Curr Opin Neurol 2018;31:36-43.

**Cite this article as:** Han X, Wang Y, Chen Y, Qiu Y, Gu X, Dai Y, Xu Q, Sun Y, Zhou Y. Predicting white-matter hyperintensity progression and cognitive decline in patients with cerebral small-vessel disease: a magnetic resonance-based habitat analysis. Quant Imaging Med Surg 2024;14(9):6621-6634. doi: 10.21037/qims-24-238

 